Cellular/Molecular

Networks of Parvalbumin-Positive Interneurons in the Basolateral Amygdala

Alan R. Woodruff and Pankaj Sah
Queensland Brain Institute and School of Biomedical Sciences, The University of Queensland, Brisbane, Queensland 4072, Australia

The amygdala is a temporal lobe structure that is required for processing emotional information. Polymodal sensory information enters the amygdala at the level of the basolateral amygdala (BLA) and undergoes local processing, after which the behavioral and autonomic responses that accompany emotions are initiated. Two main neuron types are present in the BLA, pyramidal-like principal neurons that use glutamate as their transmitter, and local circuit interneurons that use GABA as their transmitter. Although the properties of principal neurons are known in some detail, very little is known about the properties of BLA interneurons or the local circuits in which they are involved. Using mice in which EGFP (enhanced green fluorescent protein) is expressed under the control of the parvalbumin promoter, we characterized the properties of parvalbumin-positive interneurons in the BLA. By making recordings from interneuron–interneuron and interneuron–principal neuron pairs, we analyzed the intrinsic circuitry of the BLA. We show that parvalbumin-positive interneurons can be divided into four subtypes as defined by their firing properties. Interneurons are electrically coupled in subtype-specific networks and exhibit subtype-specific heterogeneities in their synaptic dynamics and patterns of connectivity. We propose that these properties allow networks of parvalbumin-expressing neurons to perform an array of information-processing tasks within the BLA.

Key words: **oscillations; fear; network; fear; learning; LTP**

Introduction

The amygdaloid complex is a structure in the mid-temporal lobe that plays a key role in processing emotional information (LeDoux, 2000; Davis and Whalen, 2001; Sah et al., 2003). The main input nucleus of the amygdala is the basolateral amygdala (BLA), a cortical-like structure in which two main types of neuron have been described: glutamatergic principal neurons and GABAergic interneurons (McDonald, 1992; Smith et al., 1998). Principal neurons, which are similar to pyramidal neurons in the hippocampus and cortex, constitute the majority (85–90%) of the BLA neuronal population (McDonald, 1992) and display a variety of firing properties (Sah et al., 2003). Although less numerous than their glutamatergic counterparts, GABAergic interneurons are imposingly diverse. These neurons have been studied in detail in the hippocampus and cortex, where this diversity is seen at almost every level, from morphological differences in dendritic and axonal arborization to differential expression of voltage-gated channels, ligand-gated receptors, and neurochemical markers (Freund and Buzaki, 1996; Markram et al., 2004). Recent studies have found that interneurons can be separated into distinct classes based on physiological and morphological criteria. Interneurons that fall into a particular class can be distinguished on the properties and dynamics of both synaptic inputs and outputs (Beierlein et al., 2003) and selectively couple to each other both synaptically and electrically via gap junctions (Hestrin and Galarreta, 2005). It has therefore been suggested that populations of interneurons within the cortex and hippocampus are coupled in separate networks that play distinct roles in information processing (Markram et al., 2004; Hestrin and Galarreta, 2005).

Four populations of interneurons have been described in the BLA: those expressing parvalbumin (McDonald, 1992; McDonald and Betette, 2001), those expressing somatostatin (McDonald and Mascagni, 2002), those expressing cholecystokinin and either calretinin or vasoactive intestinal peptide (Mascagni and McDonald, 2003), and those expressing cholecystokinin but not calretinin or vasoactive intestinal peptide (Mascagni and McDonald, 2003). Of these, parvalbumin-containing (PV+) neurons form ~50% of the interneuronal population, showing extensive colocalization with calbindin (McDonald and Betette, 2001), but not expressing the other markers. Electrophysiological recordings from interneurons in the BLA both *in vitro* (Rainnie et al., 1993, 2006; Mahanty and Sah, 1998) and *in vivo* (Lang and Pare, 1998) have also revealed a diversity of firing properties. However, little is known about the identity of these interneurons or their connectivity.

In this study, we examined the properties of parvalbumin-expressing interneurons in the basal amygdala. By recording from cells expressing enhanced green fluorescent protein (EGFP) under the control of the parvalbumin promoter (Meyer et al., 2002), we show that parvalbumin-expressing interneurons can be separated into four different classes based on their firing properties. Using paired recordings from interneuron-interneuron (IN–IN) pairs, we show that electrical coupling exists between PV-interneurons, and preferentially occurs between interneu-

Received Aug. 24, 2006; revised Dec. 11, 2006; accepted Dec. 12, 2006.

This work was supported by grants from the National Health and Medical Research Council of Australia and the Australian Research Council. We thank Rowan Tweedale for comments on this manuscript.

Correspondence should be addressed to Pankaj Sah, Queensland Brain Institute, The University of Queensland, Brisbane, Queensland 4072, Australia. E-mail: pankaj.sah@uq.edu.au.

DOI:10.1523/JNEUROSCI.3686-06.2007

 0270-6474/07/270553-11$15.00/0

rons of the same class, whereas recordings from interneuron–principal neuron (IN–PN) pairs demonstrate that PV-interneurons in the BLA exhibit considerable heterogeneity in their synaptic connectivity and dynamics. These results indicate the presence of distinct PV-IN networks within the BLA that are suited for different intra-amygdaloid processing tasks.

Materials and Methods

Coronal brain slices containing basolateral amygdala were cut from 16- to 25-d-old mice that expressed EGFP under the control of the parvalbumin promoter (Meyer et al., 2002). Heterozygous PV-EGFP animals were bred with BALB/c mice and PV-EGFP-positive animals identified by examining the fluorescence in skeletal muscle on their ears using a UV lamp. After halothane anesthesia, animals were decapitated, and the brain was rapidly removed and placed in ice-cold, oxygenated artificial CSF containing the following (in mM): 118 NaCl, 2.5 KCl, 2.5 $NaHCO_3$, 10 glucose, 1.3 $MgCl_2$, 2.5 $CaCl_2$, and 1.2 NaH_2PO_4. Slices were cut (300 μm) and incubated at 32°C for 30 min before being allowed to equilibrate at room temperature for at least an additional 30 min. All procedures were approved by the University of Queensland Animal Ethics Committee.

During recording, slices were perfused with heated artificial CSF (34 ± 2°C). Recording pipettes (3–5 MΩ) fabricated from borosilicate glass were filled with a solution containing the following (in mM): 135 $KMeSO_4$, 8 NaCl, 10 HEPES, 2 Mg_2ATP, 0.3 Na_3GTP, 0.1 spermine, 7 phosphocreatine, and 0.3 EGTA. Visualization of PV-EGFP neurons was achieved using an upright microscope (Olympus BX50WI; Olympus Optical, Tokyo, Japan) equipped with a fluorescence attachment. In some experiments, either Alexa 594 (20 μM) or Neurobiotin (2%) was also included in the internal solution, and after recordings, cells were either imaged on a Zeiss 510 multiphoton imaging system in which *z*-stacks were obtained to determine cell morphology or processed for Neurobiotin staining using a commercially available avidin–biotin complex (ABC) kit, and then drawn using a Neurolucida system (see supplemental data, available at www.jneurosci.org as supplemental material). Paired whole-cell recordings were made using Axopatch 1D and Axopatch 200B amplifiers (Molecular Devices, Foster City, CA), filtered at 5 kHz and digitized at 10 kHz using an ITC-16 board (InstruTech, Port Washington, NY). Analysis was performed using Axograph 4.6 or 4.9 (Molecular Devices).

Cells included in this study were restricted to those exhibiting an initial resting membrane potential more hyperpolarized than −55 mV. Immediately after breakthrough, cells were injected with 600 ms current pulses (−100 to 700 pA; 50 pA increments) to confirm interneuron or principal neuron identity. Plots of instantaneous spike frequency were derived from traces in which cells were subjected to twice-threshold current injections. For paired recordings, the presynaptic cell was injected with a 2 ms, 2 nA current to evoke an action potential. For voltage-clamp recordings, the postsynaptic cell was held at −60 mV for AMPA/kainate currents and at −40 mV for $GABA_A$ currents. Unitary postsynaptic current latency was measured from the peak of the presynaptic action potential to the onset of the postsynaptic event. Amplitudes of unitary IPSCs (uIPSCs) and unitary EPSCs (uEPSCs) were calculated by averaging all responses (including failures). The presence or absence of electrical coupling was determined via injection of subthreshold depolarizing or hyperpolarizing currents (50–100 ms duration; 75–200 pA). The strength of coupling was quantified by calculation of the coupling coefficient, defined as the ratio of the voltage change in the noninjected cell to that in the injected cell. Gap junction filtering characteristics were assessed using sinusoidal current waveforms of varying frequency (1–50 Hz) injected into one of the two coupled cells.

Immunocytochemistry. For neurons filled with Neurobiotin, slices were fixed overnight in 4% paraformaldehyde and resectioned at 100 μm. Neurons were visualized using the avidin–biotinylated horseradish peroxidase reaction with nickel intensification (Vectastain ABC Elite kit; Vector Laboratories, Burlingame, CA). Slices were soaked overnight in avidin-horseradish peroxidase. After washing in Tris buffer (0.1 M; pH 7.4), filled cells were visualized using the diaminobenzidine procedure. Slices were then mounted on albumin-coated slides, dried overnight, dehydrated in an ascending series of alcohols, cleared in xylene, and coverslipped in Permount. For immunohistochemistry, slices were permeabilized in blocking buffer (PBS plus 0.1% Triton X-100, 2% fetal calf serum, 2% goat serum, 2% BSA) for 30 min, and then incubated overnight at 4°C with a mouse monoclonal parvalbumin antibody (Sigma-Aldrich, St. Louis, MO) (1:2000 dilution in blocking buffer). Incubated slices were washed three times for 15 min in PBS, and then incubated at room temperature for 1 h in Alexa Fluor 350-conjugated goat anti-mouse IgG (H+L; 1:1000 in blocking buffer; Invitrogen, San Diego, CA) and streptavidin Alexa Fluor 568 (1:500 in blocking buffer; Invitrogen). Slices were washed three times for 15 min in PBS, and then briefly in distilled water before being transferred to slides, where they were mounted in fluorescent mounting medium (DakoCytomation, Carpinteria, CA), coverslipped, and analyzed using an upright fluorescence microscope (Zeiss Axioplan 2; Zeiss, Göttingen, Germany).

Results

Identification and classification of PV+ interneurons

Whole-cell recordings were made from cells expressing EGFP under the control of the parvalbumin promoter (Fig. 1*A*) (Meyer et al., 2002). The original description of mice expressing EGFP under the control of the parvalbumin promoter described some mouse lines in which multiple copies of the transgene were integrated. In these lines, there was only 60% colocalization of EFGP and parvalbumin (Meyer et al., 2002). We have not quantified the number of copies of the transgene in our strain. However, colocalization of EGFP and parvalbumin was seen in 78 ± 2% ($n = 3$) of neurons in the basal nucleus (supplemental Fig. 1, available at www.jneurosci.org as supplemental material) and all four cells types we describe expressed both GFP (green fluorescent protein) and parvalbumin (Fig. 1*F*), indicating that all cell types are indeed parvalbumin-positive interneurons. These neurons were generally aspiny and did not show any obvious morphological differences (supplemental Fig. 2, available at www.jneurosci.org as supplemental material). A recent study has suggested that parvalbumin-positive interneurons in the rat BLA undergo significant developmental changes in their distribution and morphology between the ages of postnatal day 21 (P21) and P30 (Berdel and Morys, 2000). Our studies have been limited to animals aged P16–P25 with most experiments being done on animals aged around P16–P18. In PV-EGFP mice, there was no obvious change in the distribution of EGFP-positive neurons over these ages. This may be a species difference; however, we cannot rule out the possibility that there may be additional developmental changes in the properties we describe with development.

The presence of mRNA for parvalbumin in ~7% of projection neurons in the BLA was recently reported based on single-cell PCR (Sosulina et al., 2006). However, the presence of parvalbumin was not confirmed in these neurons. In the present study, all EGFP-positive neurons were electrophysiologically confirmed as interneurons (Gupta et al., 2000) based on their firing properties and spontaneous activity on entering whole-cell mode. Thus, EGFP-positive cells fired short duration action potentials with a half-width of 0.51 ± 0.01 ms ($n = 158$), in contrast to principal cells that had action potentials with a half-width of 0.97 ± 0.06 ms ($n = 14$; $p < 0.001$). As previously shown for interneurons in the lateral amygdala (Mahanty and Sah, 1998), all EGFP-positive cells also exhibited larger, faster, and more frequent spontaneous EPSCs (sEPSCs) compared with pyramidal neurons. At a holding potential of −60 mV, the amplitude and decay time constant of sEPSCs in interneurons were 24.6 ± 2.4 pA and 2.3 ± 0.1 ms, respectively ($n = 17$), compared with those recorded from pyra-

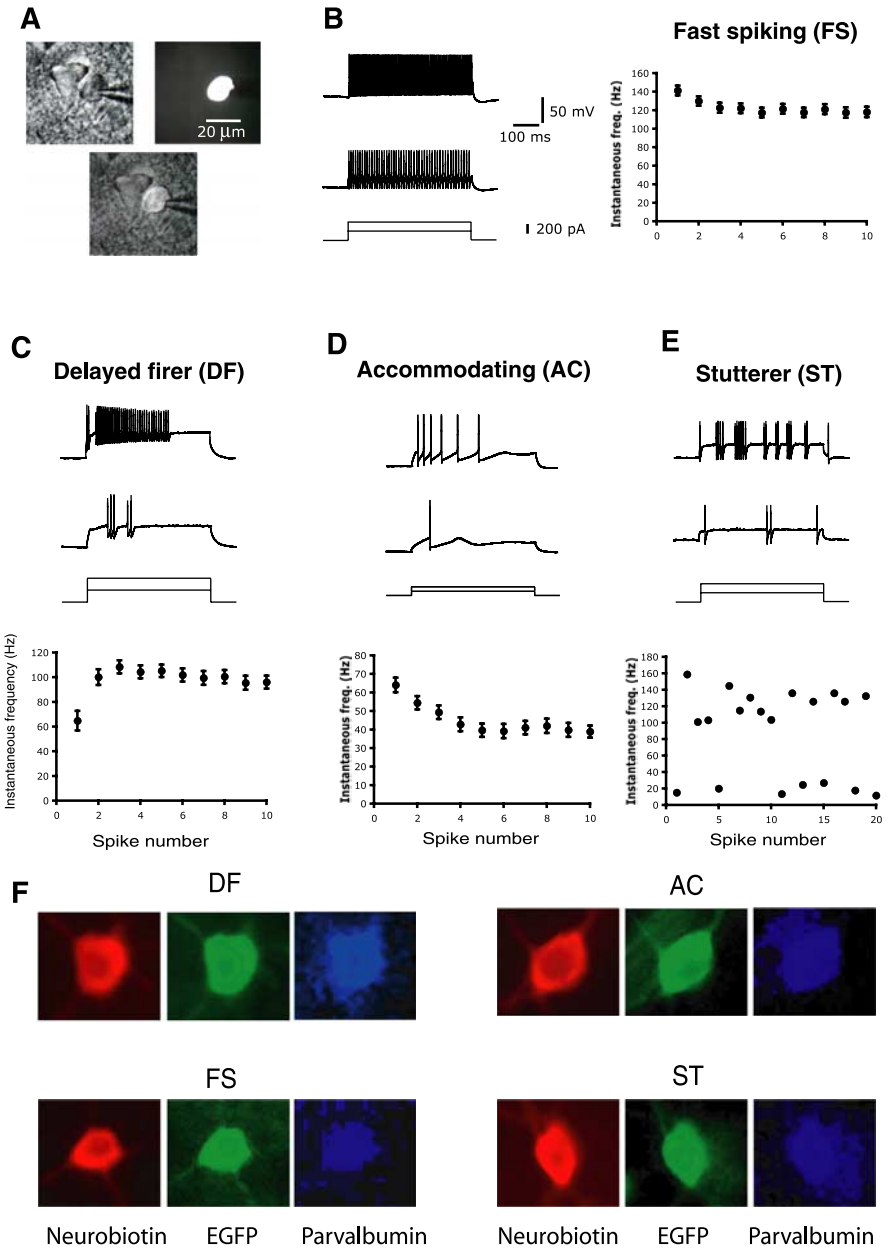

Figure 1. Four types of parvalbumin-expressing interneurons in the BLA. ***A***, Identification of PV-positive interneurons of the BLA. Infrared differential interference contrast (left) and fluorescence (right) images showing recording from a PV+ interneuron. Overlay is shown at the bottom. ***B–E***, Representative traces showing firing properties of interneurons in response to 600 ms depolarizing current injections at threshold and twice threshold. The graphs on the right in each panel show average instantaneous spike frequency at twice threshold current injection. ***B***, FS neurons fire at high frequency throughout the current injection with little accommodation. ***C***, DF neurons show a delay before the first action potential for threshold current injections, and then spike at high frequency. ***D***, AC neurons show marked spike frequency adaptation. ***E***, ST neurons fire action potentials in high-frequency bursts with variable interburst intervals. Instantaneous spike frequency plot is shown for a single cell because of variability in the interburst interval. Error bars indicate SEM. ***F***, Electrophysiologically identified neurons express parvalbumin. In each case, neurons that have been identified electrophysiologically were filled with Neurobiotin, and then fixed and processed for Neurobiotin and parvalbumin immunohistochemistry.

midal neurons: amplitude, 16.8 ± 1.0 pA ($n = 13$; $p < 0.05$), and decay time constant, 4.0 ± 0.2 ms ($n = 13$; $p < 0.001$). Furthermore, as described previously (Mahanty and Sah, 1998), the AMPA components at synaptic inputs to all EGFP-positive cells displayed clear inward rectification (data not shown) consistent with these receptors lacking glutamate receptor 2 (GluR2) subunits, typical for these receptors in interneurons.

In response to depolarizing current injections, EGFP-positive cells could be separated into four distinct types based on their firing properties (Fig. 1). We denoted these subtypes as fast spiking (FS), delayed firing (DF), accommodating (AC), and stuttering (ST). Electrophysiological recordings from BLA neurons both *in vivo* (Lang and Pare, 1998) and *in vitro* (Washburn and Moises, 1992; Mahanty and Sah, 1998) have previously found that interneurons fire narrow action potentials that show little accommodation with long current injections. Although these cells were not identified according to the presence of calcium-binding proteins, their firing properties are in general similar to those of the cells we characterized as FS. A stuttering phenotype has also been previously reported in the BLA (Washburn and Moises, 1992) and neurons with similar properties have more recently been shown to express parvalbumin (Rainnie et al., 2006).

In our sample, FS cells (75 of 158) (Fig. 1*B*) were the most common cell type, contributing 47% of the cells included in this study. These cells had action potential half-widths of 0.47 ± 0.01 ms and, in response to long (600 ms) current injections, discharged at high frequency with little or no spike frequency adaptation as can be seen in the plot of instantaneous frequency against spike number (Fig. 1*B*). DF cells (Fig. 1*C*), which formed 22% (35 of 158) of PV-positive interneurons, had action potential half-widths of 0.52 ± 0.02 ms and displayed a delayed action potential initiation at threshold. This is reflected in the significantly longer latency to first spike for these neurons compared with FS and AC neurons (Table 1). In response to depolarizing current injections, DF cells exhibited a marked depolarizing ramp at the onset of spike initiation (Fig. 1*C*). For larger current injections, DF cells fired one or two action potentials at high frequency and, after a clear delay, fired additional nonaccommodating trains of high-frequency spikes. Notably, DF cells appeared to have a slightly more depolarized spike threshold (Table 1). AC cells (Fig. 1*D*) formed 21% (33 of 158) of the PV-interneuron population and had significantly broader action potentials (half-width, 0.61 ± 0.02 ms; $n = 33$) than those of the other interneuron types. In response to larger current injections, these cells spiked at significantly lower frequencies than other interneurons, and showed clear spike frequency adaptation during prolonged current injection. ST cells (Fig. 1*E*) were the least common class of PV-positive interneurons, forming 10% (15 of 158) of the population. These cells had action potential half-widths of 0.49 ± 0.02 ms and were characterized by bursts of high-frequency spikes (~130 Hz) separated by variable interburst intervals. These bursts are similar to

those seen with threshold current injections in DF neurons (Fig. 1*C*); however, in ST neurons, this "stuttering" behavior continued with larger current injections (Fig. 1*E*), whereas DF neurons fired a continuous high-frequency train (Fig. 1*C*). Furthermore, the depolarizing ramp seen in DF cells at smaller injection levels was not present in ST cells. The presence of these high-frequency bursts precluded averaging the response to higher current injections as shown for the other cell types in Figure 1. The electrotonic properties of the four cell types are summarized in Table 1.

Thus, on the basis of their firing properties, neurons that express parvalbumin can be separated into four distinct classes. To determine whether these four groups are heterogeneous in their synaptic and electrical connectivity, simultaneous dual whole-cell recordings were made from pairs of PV-interneurons (IN–IN pairs) and from PV-interneuron and principal neuron pairs (IN–PN). All recorded pairs had somata within 120 μm of each other.

Table 1. Electrotonic properties of four types of parvalbumin-expressing interneurons in the basolateral amygdala: FS, DF, AC, and ST

	FS	DF	AC	ST
Threshold (mV)	-34.9 ± 0.5*	$-28.8 \pm 0.5^{\#}$	-32.9 ± 0.6	$-32.3 \pm 0.5^{\P}$
AP half-width (ms)	$0.47 \pm 0.01^{\S}$	$0.52 \pm 0.02^{\S}$	0.61 ± 0.02	$0.49 \pm 0.02^{\S}$
Input resistance (MΩ)	184.4 ± 10.2	172.1 ± 23.7	218.1 ± 13.7	$157.2 \pm 14.3^{\#}$
Membrane time constant (ms)	$13.4 \pm 0.7^{\S}$	$14.2 \pm 1.0^{\S}$	23.0 ± 1.4	$14.6 \pm 1.5^{\S}$
Latency to first spike (ms)	$11.2 \pm 2.2^{\S*¤}$	$108.2 \pm 12.1^{\S}$	46.6 ± 6.4	$116.8 \pm 28.8^{\#}$

AP, Action potential. $^{\#}p < 0.01$ versus AC; $^{\S}p < 0.001$ versus AC; $^{\P}p < 0.05$ versus DF; $^{*}p < 0.001$ versus DF; $^{¤}p < 0.001$ versus ST.

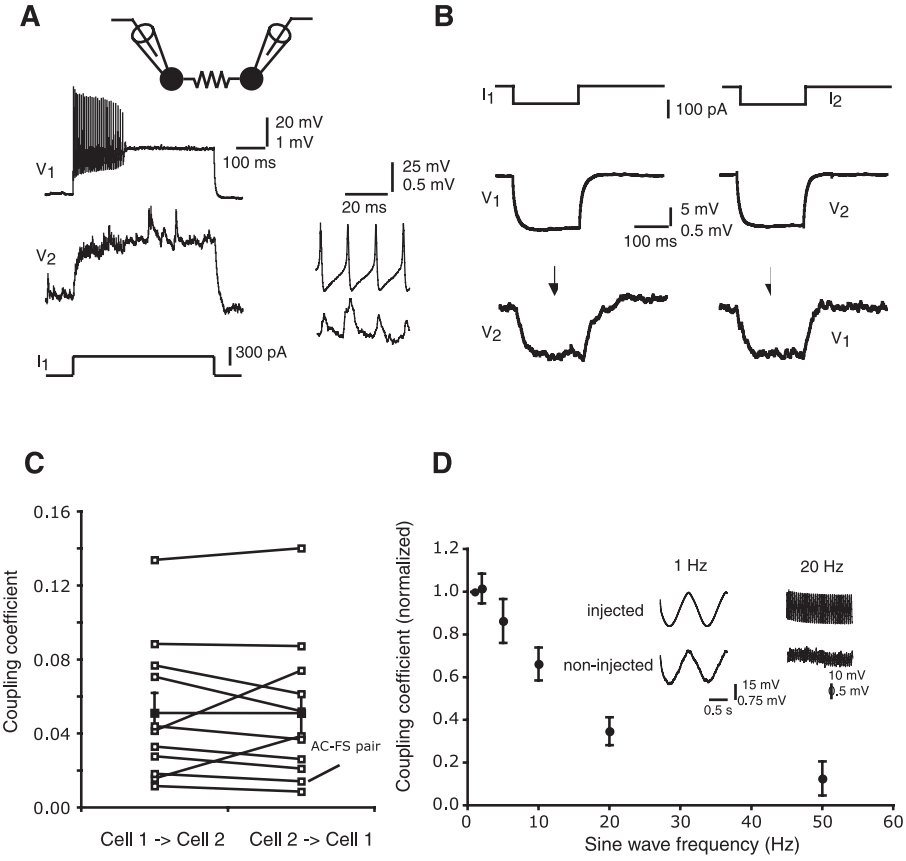

Figure 2. Parvalbumin-positive interneurons are coupled by gap junctions. ***A***, Paired recording from two EGFP-expressing interneurons. Current injected into one interneuron (left traces; I_1) causes a high-frequency discharge in that cell (V_1) that is seen in the second neuron (V_2) as a sustained depolarization superimposed on which are small amplitude spikelets time locked to action potentials in the first cell. Spikelets in V_2 and action potentials in V_1 are shown on an expanded scale in the inset. ***B***, Injection of a 600 ms hyperpolarizing current injection into cell 1 (I_1) causes a large hyperpolarization in cell 1 (V_1) that is transmitted as a much reduced voltage change in cell 2 (V_2; traces on left). Similarly, current injection into cell 2 (I_2; right traces) leads to a large voltage change in cell 2 (V_2) and a reduced voltage change in cell 1 (V_1). ***C***, Coupling coefficients in both directions are plotted for all pairs that were electrically coupled. ***D***, Low-pass filter characteristics of gap junctions. Sine wave currents of different frequencies were injected into one coupled cell and voltage responses recorded in both. The inset shows traces from two frequencies, demonstrating decreased coupling at higher frequencies. Error bars indicate SEM.

Electrical coupling among PV-positive interneurons

Recent studies have demonstrated that cortical and hippocampal interneurons are electrically coupled via gap junctions (Galarreta and Hestrin, 1999; Gibson et al., 1999; Bartos et al., 2001). This electrical coupling is mostly restricted to interneurons of the same electrophysiological class (Hestrin and Galarreta, 2005). In the BLA, morphological analysis has demonstrated the presence of dendro-dendritic gap junctions between PV-positive interneurons (Muller et al., 2005). We therefore tested whether these electrical connections are restricted within the four classes of PV-positive interneurons in the BLA.

To test for the presence of electrical coupling, paired recordings were made from IN–IN pairs ($n = 140$ pairs), and depolarizing and hyperpolarizing current pulses were injected into one of the cells. Coupling could be detected both by the presence of coupled depolarization, and spikelets, in the coupled neurons (Fig. 2*A*) after suprathreshold depolarizing current injections, and by injection of hyperpolarizing current, which revealed a voltage change in the noninjected neuron (Fig. 2*B*). From 140 paired recordings, electrical coupling was detected on 11 occasions (8%). Electrical connections between all pairs were bidirectional, with coupling coefficients being similar regardless of which cell was designated presynaptic or postsynaptic (0.05 ± 0.01 vs 0.05 ± 0.01; $n = 11$; $p = 0.98$) (Fig. 2*C*) and behaved as low-pass filters attenuating high-frequency signals (Galarreta and Hestrin, 1999) (Fig. 2*D*). As for interneurons in other brain regions (Hestrin and Galarreta, 2005), we found that coupling between pairs of the same electrophysiological subtype ("like pairs") occurred with far greater likelihood than for "unlike" pairs (Fig. 3). We recorded from like pairs on 22 occasions and found that 10 of these, or 45.5%, were coupled (four FS–FS; three DF–DF; two AC–AC; one ST–ST). The remaining 118 IN–IN recordings, from "unlike pairs," resulted in just one instance of electrical coupling (1 of 118, 0.8%; AC–FS pair). Thus, electrical coupling in the BLA occurs preferentially between pairs of interneurons exhibiting similar firing properties (Fig. 3*E*), consistent with our division of PV-interneurons in the basolateral amygdala into four distinct groups.

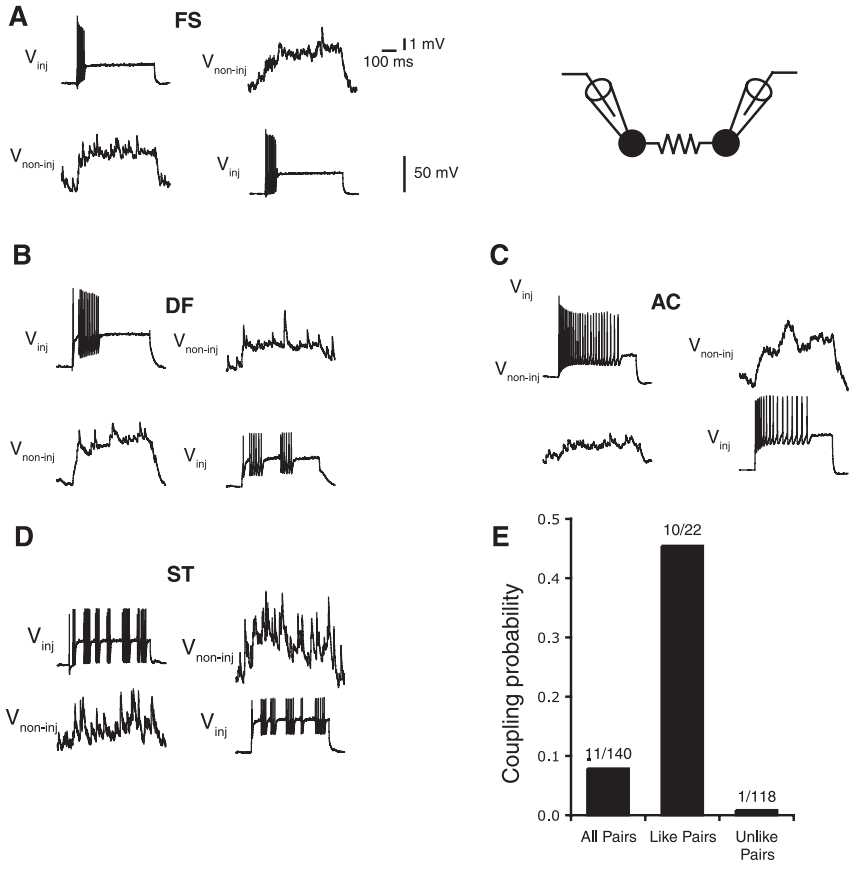

Figure 3. Electrical coupling occurs preferentially between interneurons of the same class. Paired recordings were made from two EGFP-expressing interneurons. ***A–D*** show recordings from pairs in which the two cells were of the same phenotype. In each panel, traces on the top left show the response of cell 1 to a twice threshold current injection and the bottom traces show the voltage response in the uninjected cell. Traces on the right show the reverse situation with current injected current into cell 2. Gap junctional coupling is preferentially between cells with similar firing properties. The histograms in ***E*** show the probability of coupling between similar cells and cells with different firing properties.

Synaptic interneuron/interneuron connections

We next tested for chemical connections between interneurons by evoking action potentials with brief (2 ms) suprathreshold current injection into one neuron of a paired recording. In synaptically connected pairs, an action potential in the presynaptic cell evoked a time-locked inhibitory synaptic potential in the postsynaptic neuron (Fig. 4*A*). Of the 140 paired IN–IN recordings, 28 pairs had a unidirectional synaptic connection and 4 pairs had bidirectional connections, giving an overall connection probability of 26% (36 of 140). Twenty-five of these pairs were tested under voltage-clamp conditions. uIPSCs recorded in interneurons had an average failure rate of 24 ± 5%, and a peak amplitude of 31.2 ± 7.4 pA (V_h, −40 mV; $n = 25$). uIPSCs were abolished by application of bicuculline (Fig. 4*B*) ($n = 4$), confirming mediation by $GABA_A$ receptors. When two action potentials were evoked with a separation of 50 ms, the majority (22 of 25) of IN→IN synapses exhibited paired-pulse depression (Fig. 4*C*), with the average paired-pulse ratio (PPR) being 0.79 ± 0.03. The remaining three connections only slightly facilitated (PPR range, 1.09–1.13). Although differences in connectivity preferences were observed (see below), no subtype-specific differences in synaptic properties were found after arranging pairs according to either presynaptic or postsynaptic phenotype. uIPSCs recorded in interneurons had 10–90% rise times of 1.1 ± 0.1 ms and their decay was well fitted by a single exponential with an average time constant of 6.8 ± 0.4 ms ($n = 25$). As reported previously with extracellular stimulation in amygdala interneurons (Martina et al., 2001), no $GABA_B$ response could be elicited in the postsynaptic cell on tetanic stimulation.

As for cortical interneurons (Galarreta and Hestrin, 1999), PV-positive interneurons connected by gap junctions could also form conventional GABAergic synapses with each other. Thus, an action potential in one cell resulted in a voltage response in the connected cell consisting of the propagated fast depolarizing spikelet and slow afterhyperpolarization and the synaptically mediated IPSC (Fig. 4*D*). As expected, during trains of action potentials, the $GABA_A$-mediated connection runs down as release probability decreases, whereas the spikelet that is transmitted via the gap junction is unaffected (Fig. 4*D*, bottom trace). It was notable that the onset of the $GABA_A$-mediated conductance occurred with sufficient speed to shorten the window of depolarization provided by the coupled spikelet (Fig. 4*D*). This result suggests that interneurons communicating via both GABAergic and electrical synapses will synchronize their activity more effectively than those connected by purely electrical means. We tested 8 of the 11 electrically coupled pairs for the presence of a chemical connection and found that 6 demonstrated a $GABA_A$-mediated current when the postsynaptic cell was voltage clamped at −40 mV. Of these six pairs, two formed reciprocal GABAergic connections with each other. Thus, neurons that are electrically coupled have a significantly higher probability of forming GABAergic connections with each other than for uncoupled neurons. The probability of a unidirectional connection between coupled neurons was 50% compared with 19% between uncoupled neurons ($p < 0.02$), whereas the probability of a bidirectional connection was 25% for coupled neurons compared with 3% for uncoupled neurons ($p < 0.001$) (Fig. 4*E*). These results indicate that synaptic connectivity among interneurons is not random but rather depends on whether the cells form part of the same electrically coupled network.

PV-positive interneuron–principal neuron connections

To examine the effects of the inhibitory circuitry in the BLA, recordings were made from 160 IN–PN neuron pairs. Of these, 99 exhibited synaptic connections, with 34% (55 of 160) forming a unidirectional IN→PN inhibitory connection, 12% (19 of 160) showing an unreciprocated PN→IN excitatory connection, and 16% (25 of 160) being reciprocally connected. The remaining 38% (61 of 160) of IN–PN pairs were not connected in any way. We did not observe any difference between uIPSCs or uEPSCs recorded in reciprocated versus unreciprocated pairs, and have therefore pooled these data for analysis.

Interneuron to principal neuron connections

In IN→PN connections, action potentials evoked in the interneuron elicited a time-locked hyperpolarizing response in the

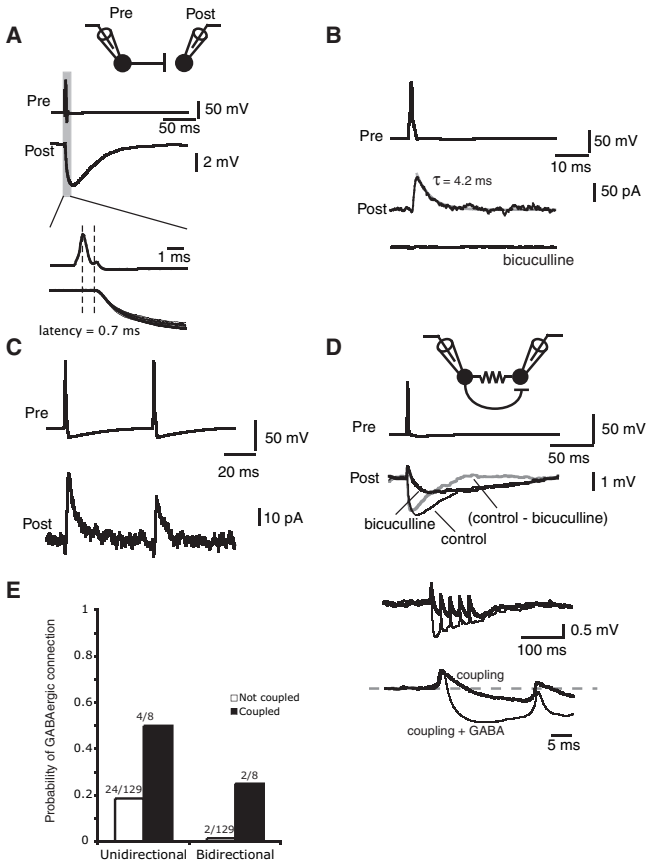

Figure 4. Parvalbumin-expressing interneurons are connected both electrically and chemically. Paired recordings were made from two EGFP-expressing interneurons. ***A***, PV-positive interneurons form monosynaptic connections with each other. The action potential evoked in cell 1 (pre) by a suprathreshold current injection (2 ms) leads to an IPSP in cell 2 (post; top traces). The bottom traces are 10 overlaid traces that show the connection has a low failure rate and a synaptic response latency of 0.7 ms. ***B***, Postsynaptic currents exhibit rapid kinetics and are mediated purely by $GABA_A$ receptors. When the postsynaptic cell is voltage clamped (V_h, −40 mV), an action potential in the presynaptic cell evokes an outward current in the postsynaptic cell that has rapid decay kinetics. The outward current is abolished by the $GABA_A$ receptor antagonist bicuculline (10 μM). ***C***, Synaptic IN→IN connections show paired-pulse depression. The response of the postsynaptic cell to two action potentials separated by 50 ms shows that the second IPSC has a smaller amplitude than the first. ***D***, Interneurons coupled by gap junctions can also form chemical synapses. An action potential evoked in one interneuron evokes a spikelet followed by a slower hyperpolarizing response. Application of the $GABA_A$ receptor antagonist bicuculline (10 μM) blocks the fast component of the hyperpolarizing response. The traces below show the postsynaptic response to a train of action potentials before and after blockade of the synaptic IPSP with bicuculline. Note that, in response to a train of action potentials, the postsynaptic response shows an IPSP that depresses in amplitude, whereas the spikelet amplitude remains unaffected. The expanded traces below show that the synaptic IPSP curtails the spikelet. ***E***, Interneurons that are coupled by gap junctions have a higher probability of being synaptically connected.

postsynaptic principal neuron. These connections were monosynaptic, as determined by their response latencies (0.50 ± 0.04 ms; $n = 31$; range, 0.3–1 ms) (Fig. 5*A*) and were abolished by the $GABA_A$ receptor antagonist bicuculline (10 μM) (Fig. 5*B*) ($n = 4$). Under our recording conditions, these inputs had a reversal potential near the chloride reversal potential (Fig. 5*C*).

Under voltage clamp, at a holding potential of −40 mV, average uIPSC amplitudes recorded in principal neurons ranged from 28.1 ± 6.1 pA for ST cells ($n = 6$) to 41.8 ± 6.8 pA for FS cells ($n = 29$). These connections were highly reliable, with failure rates ranging from 13 ± 3% (DF; $n = 30$) to 4 ± 2% (AC; $n = 7$) and, as for IN→IN connections (Fig. 4), depressed with repetitive activity (PPR range, 0.71 ± 0.02 for DF cells, $n = 30$; 0.81 ± 0.09 for AC cells, $n = 7$). Although these parameters varied little between subtypes, significant kinetic heterogeneities were apparent. Activation of DF and FS cells gave rise to uIPSCs with rapid kinetics. The 10–90% rise times for these inputs were 1.3 ± 0.1 ms ($n = 30$) and 1.3 ± 0.1 ms ($n = 29$), respectively, whereas their decay time constants were 10.6 ± 0.5 and 10.9 ± 0.7 ms, respectively (Fig. 5*D*,*E*). In contrast, both the rise time and decay time constant were significantly slower ($p < 0.05$) for AC cells, which evoked uIPSCs with a 10–90% rise time of 2.1 ± 0.2 ms and a decay time constant of 13.7 ± 1.6 ms ($n = 7$) (Fig. 5*D*,*E*). The physiological properties of IN→PN connections are summarized in Table 2. The kinetic differences between IPSCs generated by the different cell types suggest that axons of DF and FS cells may preferentially target more proximal regions of principal cells compared with the axons of AC cells. Consistent with this, ultrastructural studies have shown that a substantial proportion of PV+ terminals in the basal amygdala target principal neuron distal dendrites (Smith et al., 1998; McDonald et al., 2005), and it has been estimated that up to 40% of calbindin-expressing interneurons in the rat basolateral nucleus, the majority of which are likely to also express parvalbumin, target distal principal neuron dendrites (Muller et al., 2003). It therefore seems likely that these dendrite targeting interneurons express parvalbumin. It was notable that uIPSCs in interneurons decayed significantly faster ($\tau = 6.8 \pm 0.4$ ms) than those recorded in principal neurons (11.1 ± 0.4 ms; $n = 70$; $p < 0.001$). This is likely to be attributable to expression of different $GABA_A$ receptor subunits in interneurons compared with principal cells (McDonald and Mascagni, 2004).

Principal neuron to interneuron connections

In the BLA, 44 PN–IN pairs had excitatory connections in which action potentials in the principal neuron evoked an excitatory synaptic potential in the postsynaptic interneuron. All excitatory connections were monosynaptic, with a latency of 0.61 ± 0.04 ms (Fig. 6*A*). As expected from the voltage dependence of the NMDA receptor, at −60 mV, uEPSCs were mediated purely by AMPA/kainate receptors and were fully abolished by application of 10 μM CNQX (Fig. 6*B*). Under voltage clamp at a holding potential of −60 mV, the uEPSCs were well fitted by a monoexponential function with a decay time constant of 2.6 ± 0.2 ms ($n = 38$), consistent with the lack of GluR2-containing AMPA receptors in interneurons (Mahanty and Sah, 1998).

The strength of excitation varied widely between pairs (range, 9–380 pA). We found that AC cells received significantly weaker excitation than their counterparts (Fig. 6*C*), with the average uEPSC amplitude being just 19 ± 5 pA ($n = 6$). In contrast, for FS cells, the average unitary EPSC amplitude was 145 ± 35 pA ($n = 11$; $p < 0.05$ vs AC); for DF cells, 110 ± 29 pA ($n = 15$; $p = 0.051$ vs AC); and for ST cells, 68 ± 18 pA ($n = 6$; $p = 0.09$ vs AC). uEPSCs recorded in AC interneurons were also slower than those in the other interneuron types, with a 10–90% rise time of 0.93 ± 0.19 and a decay time constant of 3.4 ± 0.6 ms. For comparison, the rise times for FS, DF, and ST interneurons were 0.6 ± 0.1, 0.7 ± 0.1, and 0.7 ± 0.1 ms, respectively, and their decay time constants were 2.0 ± 0.2, 2.6 ± 0.3, and 2.9 ± 0.5 ms (Fig. 6*D*). The smaller amplitude and slower kinetics of inputs to AC neurons suggest that synapses on these interneurons may be electrotonically more distant than those at other interneurons. The release probability at connections to AC cells also appeared to be lower than that for connections to other cell types, as seen by a higher failure rate at these synapses (Fig. 6*E*). Thus, whereas DF,

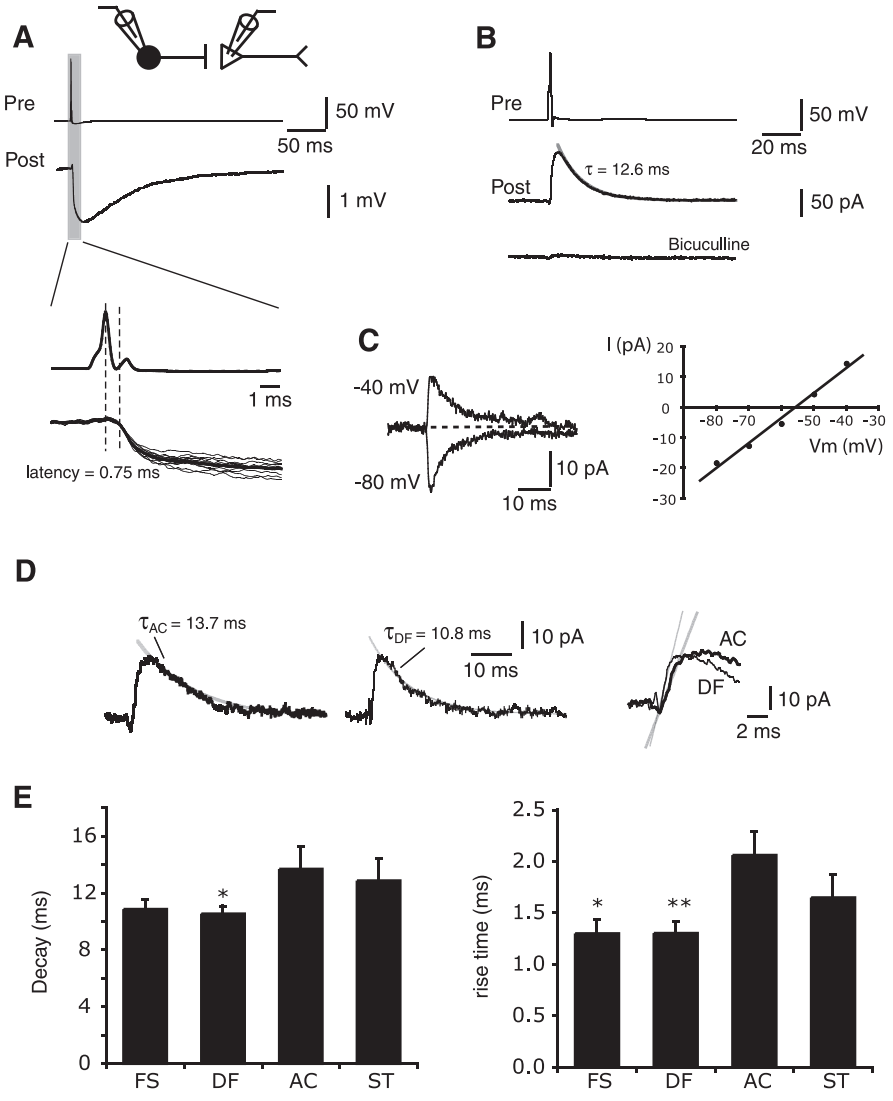

Figure 5. Parvalbumin-expressing interneuron to principal neuron connections in the BLA. ***A***, Current-clamp recording of a connected IN⟶PN pair. Current injection into the presynaptic interneuron evokes an action potential resulting in an IPSP in the postsynaptic neuron. The postsynaptic cell was held at −51 mV. Individual traces (thin) and averaged uIPSCs are shown on an expanded timescale below to demonstrate monosynaptic delay. ***B***, IPSPs are mediated by $GABA_A$ receptors. Voltage-clamp recording of an averaged uIPSC (V_h, −40 mV) with fitted monoexponential decay (gray), and after addition of 10 μM bicuculline. ***C***, IPSC reverses at the chloride equilibrium potential. IPSCs evoked at holding potentials of −40 and −80 mV have been superimposed (traces on left). The current–voltage relationship of IPSCs recorded at holding potentials of −80 to −40 mV are shown on the right. ***D***, Unitary IPSCs in AC interneurons have relatively slow kinetics. IPSCs are shown recorded from paired recordings from presynaptic AC interneuron (left) and DF interneurons (middle trace). The IPSCs have been overlaid on the right for presynaptic AC (thick trace) and DF (thin trace) cells to demonstrate the difference in rise time kinetics. ***E***, Summary data for all connected IN⟶PN pairs illustrate heterogeneous rise and decay kinetics according to IN phenotype. Error bars indicate SEM. $^*p < 0.05$; $^{**}p < 0.01$ versus AC neurons.

FS, and ST interneurons all received reliable excitation, with failure rates of 9 ± 5, 5 ± 3, and 9 ± 6%, respectively, AC interneurons received unreliable input from local principal neurons, having a failure rate of 43 ± 12% ($p < 0.01$ vs DF and FS; $p < 0.05$ vs ST). Consistent with a lower release probability, connections to AC cells showed paired-pulse facilitation with an average PPR of 1.4 ± 0.3, whereas excitatory connections to the other types of interneurons showed either paired-pulse depression or little change (Fig. 6*F*). These data show that local excitation to AC interneurons is weaker and more unreliable than that to other interneuron subtypes. Furthermore, the amplitude facilitation and slow kinetics of EPSCs at these synapses coupled with the slower membrane time constant of AC cells would lead to better temporal summation and integration of excitatory inputs during repetitive activity.

Distribution of interneuron subtypes according to synapse type

Our results show that four electrophysiologically distinct types of PV-positive interneurons can be identified within the basolateral nucleus. We demonstrated that these interneurons show subtype-specific electrical coupling and that they exhibit heterogeneities in their communication with principal (glutamatergic) neurons. A number of recent studies have found that cortical neurons are highly specific in their choice of synaptic partners (Yoshimura and Callaway, 2005; Yoshimura et al., 2005). We therefore asked whether the synaptic connectivity of PV-positive interneurons in the basolateral nucleus was determined randomly or showed subtype-specific preferences.

Interneuron–principal neuron connections

We first assessed the frequency of connections between principal neurons and each interneuron cell type. In Figure 7*A*, we plotted the frequency of each type of possible connection that we observed between interneurons and projection neurons. From this analysis, it can be seen that DF interneurons are particularly promiscuous with regard to their principal neuron connectivity, with only 14% (4 of 28) of all recorded DF–principal neuron pairs being unconnected. In contrast, AC interneurons are only sparsely connected to principal neurons, with 64% (16 of 25) of all AC–PN pairs being unconnected (Fig. 7*A*). Furthermore, it is evident that the vast majority of synaptic connections between principal neurons and PV-positive interneurons are formed by the FS and DF interneuron subpopulations.

We next assessed whether interneuron subtypes may contribute differentially to a particular type of synaptic connection. The rationale behind this was that because the four interneuron subtypes differed in the synaptic excitation they received and in the inhibition they produced, they may be suited to different roles in BLA information processing, such as feedforward or feedback inhibition. If this were the case, one might expect differences in the degree to which a particular interneuron subtype contributes to a given type of synaptic connection. We examined this by calculating the percentage contribution that each interneuron subtype provides for each type of connection ("actual" value), and comparing this to an "expected" value. The expected value was derived from the proportion that each interneuron subtype contributed to the PV-interneuron population (same cells as for data in Fig. 1) ($n = 158$) assuming

that all interneurons had an equal probability of making and receiving a connection with principal neurons. Thus, the expected values for FS, DF, AC, and ST cells were 47% (75 of 158), 22% (35 of 158), 21% (33 of 158), and 10% (15 of 158), respectively. These values are shown in the left column of Figure 7*B* (denoted "All INs").

For IN→PN connections, actual values were quite similar to expected values. FS interneurons contributed 46% (22 of 48) of all interneurons that formed IN→PN synapses, with DF, AC, and ST cells comprising 38% (18 of 48), 13% (6 of 48), and 4% (2 of 48) of this population, respectively. For excitatory PN→IN synapses, the most common interneuron subtype was the AC interneuron, although this was not statistically significant. AC interneurons comprised 36% (5 of 14) of all postsynaptic interneurons in PN→IN pairs (expected value, 21%), whereas both DF (21%; 3 of 14) and ST (14%; 2 of 14) interneurons contributed similarly to what would be expected. In contrast, AC cells were highly underrepresented in reciprocal IN↔ PN pairs (1 of 24, 4%; expected value, 21%; $p < 0.05$, χ^2 test), whereas DF cells were overrepresented, comprising 12 of 24 (50%; expected value, 22%; $p < 0.001$, χ^2 test) of all recorded pairs. Finally, the total local excitation received by FS interneurons was lower than would be expected based on their proportional representation within the PV-interneuron population. For both PN→IN and PN↔ IN synapses, which together represent the local glutamatergic excitation received by interneurons, FS interneurons were underrepresented (4 of 14 PN→IN connections, 29%; and 7 of 24 PN↔ IN connections, 29%). Although the unpooled data (PN→IN group alone and PN↔ IN group alone) are not statistically significant, pooling these two categories reveals that the total local glutamatergic excitation received by FS cells is less than would be expected by chance ($p < 0.05$, χ^2 test). These data are summarized in Figure 7*B*.

Table 2. Properties of unitary synaptic connections between parvalbumin-expressing interneurons and between interneurons and principal neurons in uIPSCs IN→PN and uEPSCs PN→IN

	FS	DF	AC	ST
uIPSCs IN→PN				
Amplitude	34.3 ± 4.6	41.5 ± 12.9	29.1 ± 8.2	36.8 ± 10.8
PPR	0.71 ± 0.02	0.71 ± 0.03	0.81 ± 0.09	0.76 ± 0.05
τ (ms)	11.3 ± 0.8	10.8 ± 0.6$^{\#}$	13.7 ± 1.6	12.0 ± 1.4
Pr	0.94 ± 0.03	0.85 ± 0.03	0.96 ± 0.02	0.89 ± 0.08
10–90% rise (ms)	1.41 ± 0.16$^{\#}$	1.29 ± 0.14§	2.06 ± 0.23	1.63 ± 0.27
uEPSCs PN→IN				
Amplitude	156.1 ± 42.4$^{\#}$	110.1 ± 28.9	19.2 ± 5.2	71.0 ± 26.8
PPR	0.90 ± 0.20	0.81 ± 0.06$^{\#}$	1.41 ± 0.30	1.03 ± 0.15
τ (ms)	1.9 ± 0.2$^{\#\P}$	2.6 ± 0.26	3.4 ± 0.6	3.2 ± 0.5
Pr	0.93 ± 0.04§	0.91 ± 0.05§	0.57 ± 0.12	0.91 ± 0.06$^{\#}$
10–90% rise (ms)	0.62 ± 0.13	0.71 ± 0.08	0.93 ± 0.19	0.71 ± 0.05

Pr, Release probability. $^{\#}p < 0.05$ versus AC; $^{\S}p < 0.01$ versus AC; $^{\P}p < 0.05$ versus ST.

Interneuron–interneuron connections

We also assessed the synaptic connectivity patterns present in IN–IN pairs. Because of limitations inherent in our sample size, we were unable to effectively determine whether any hierarchical organization existed in IN→IN communication. Instead, we organized synaptic connections on a like/unlike basis to deduce whether some interneuron subtypes preferentially connect to themselves rather than other interneuron types.

The experimental values in Figure 7*C* are represented by vertical bars. To assess the possibility of preferential connectivity among the interneuron subgroups, we performed a similar analysis to that described for IN→PN and PN→IN connections above, comparing actual to expected values. Expected values were calculated based on the percentage contribution of each interneuron subtype to the entire PV-IN population, giving expected values of 47% (FS), 22% (DF), 21% (AC), and 10% (ST). Thus, in a sample of 10 FS pairs, 4.7 (47%) connections would be expected to be between like pairs, and 5.3 (100–47%) between unlike pairs. In contrast, for DF connections, 2.2 of 10 (22%) would be expected to form between like pairs, whereas 7.8 should be between unlike pairs. These expected values are represented by dotted lines in Figure 7*C*. As can be seen, deviations from expected values are present in the FS and DF populations. These values are statistically significant when a DF cell is the presynaptic ($p < 0.01$, χ^2 test) or postsynaptic ($p < 0.01$) partner, and when an FS cell is the postsynaptic member of the pair ($p < 0.05$). In contrast, AC and ST cells show no apparent preference for like versus unlike connections. Together, these data show that FS and DF interneurons preferentially connect to themselves, forming relatively autonomous networks of interneurons.

Discussion

We examined the properties of neurons that express EGFP under the control of the parvalbumin promoter in the basolateral amygdala. Interneurons can be separated into distinct populations based on their electrophysiological properties and expression of different calcium-binding proteins and peptides (Gupta et al., 2000; Kawaguchi and Kondo, 2002; Markram et al., 2004; Hestrin and Galarreta, 2005). Within the BLA, interneurons have previously been separated into four types based initially on immunohistochemical markers (Mascagni and McDonald, 2003), but more recently on mRNA expression profiles (Sosulina et al., 2006) and electrophysiological parameters (Rainnie et al., 2006). Electrophysiological recordings from BLA interneurons expressing PV have indicated the presence of two subtypes (Rainnie et al., 2006). Burst-firing neurons were characterized by summating EPSPs, spontaneous bursts of spikes, and an accommodating firing response to prolonged current injection. Although we never observed spontaneous bursts of action potentials, such a bursting effect may result from the relatively high extracellular K^+ concentration used by Rainnie and colleagues (4.6 vs 2.5 mM). Thus, bursting neurons (Rainnie et al., 2006) may be similar to our AC cells, with the bursts arising from a combination of increased network excitability and the facilitating nature of EPSPs, characteristic of our AC cells. The second class of neurons described by Rainnie et al. (2006), termed stutter-firing neurons, shares similarities with our FS, DF, and ST classes, and may encompass all three.

We separated parvalbumin-positive neurons into four distinct groups. In addition to their differing electrophysiological properties, three lines of evidence support our proposal. First, electrical coupling between PV-interneurons shows considerable selectivity for interneuron subtype, with similar pairs being 54 times more likely to be coupled than dissimilar pairs (10 of 22 vs 1 of 118). Such subtype-specific coupling is typical for neocortical fast spiking (Galarreta and Hestrin, 1999; Gibson et al., 1999), low threshold spiking (Gibson et al., 1999), and multipolar bursting interneurons (Blatow et al., 2003), and has been proposed as a hallmark of functionally homogeneous interneuron networks

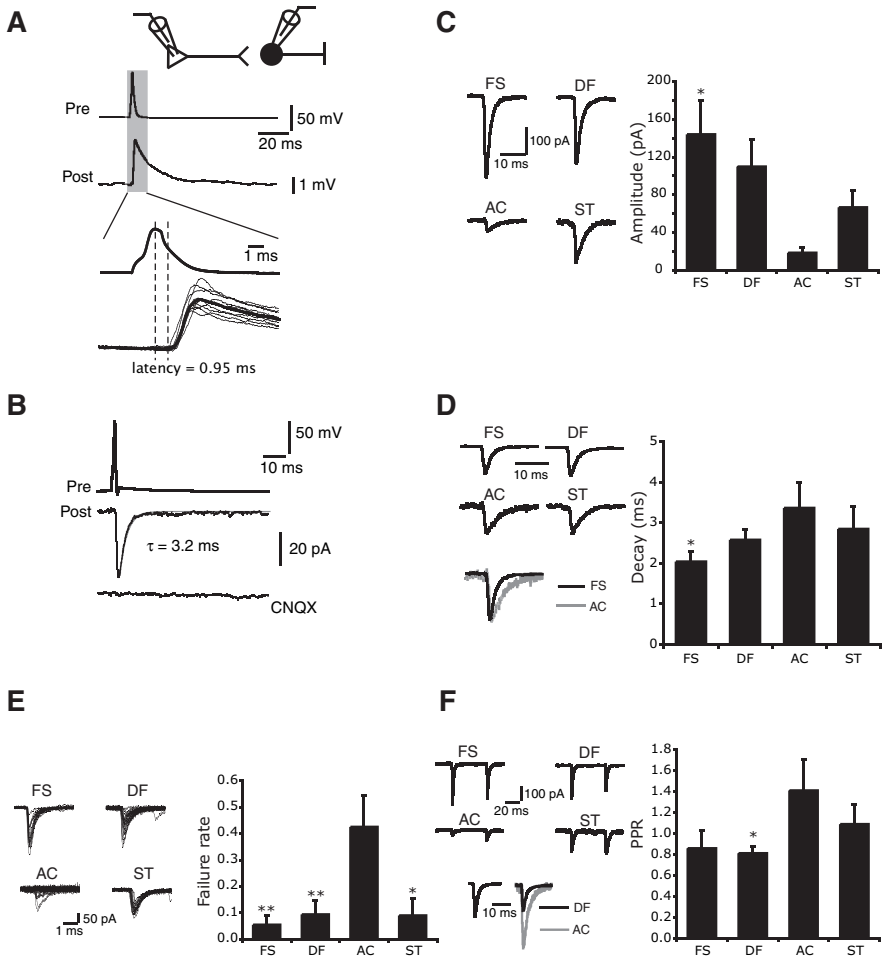

Figure 6. Principal neuron to interneuron connections in the BLA are heterogeneous. Paired recordings were made from principal neurons and EGFP-positive interneurons. ***A***, Current-clamp recording of a connected pair. An action potential evoked in the presynaptic principal neuron leads to an excitatory synaptic potential (EPSP) in the postsynaptic interneuron. Interneuron was held at −63 mV. Traces below are superimposed records on an expanded timescale showing a fixed latency EPSP that is monosynaptic. ***B***, uEPSC recorded at −60 mV is completely abolished by 10 μM CNQX. ***C–F***, EPSPs in AC interneurons are small slow and unreliable. ***C***, Shown are representative unitary EPSCs recorded at −60 mV from all four interneuron types in response to a single action potential in a principal neuron. Average data for each interneuronal type are shown on the right. ***D***, AC interneurons have EPSCs with slower decay kinetics. Normalized representative EPSCs are shown from each interneuron type in response to an action potential in a connected principal neuron. EPSCs in an AC cell (light trace) and FS cell (dark trace) are superimposed in the traces below for comparison. Average decay time constants for each interneuronal type are shown on the right. ***E***, AC interneurons receive unreliable excitation. Traces on left show superimposed responses to 20 repeated action potentials in connected principal neurons. Note the large number of failures in AC interneurons. Average failure rate for each interneuron type is plotted on the right. ***F***, Short-term dynamics of local excitation differs according to interneuron type. Representative examples of the response in different interneurons to two action potentials evoked in the connected principal neuron. EPSCs in AC cells facilitate, whereas in the other cell types the EPSCs either depress or are unchanged. The traces at the bottom show superimposed traces of the first and second EPSCs normalized to the amplitude of the first EPSC in DF (dark traces) and AC (light traces) interneurons. Error bars indicate SEM.

(Hestrin and Galarreta, 2005). Second, glutamatergic synaptic inputs to PV-interneurons show a number of properties that vary according to the interneuron subtype. Similarly, inhibition of basolateral (BL) principal neurons by PV-interneurons exhibits kinetic variability that maps well to the presynaptic interneuron type. Lastly, interneuron subtypes demonstrate a numerical preference for contributing to a particular synapse type that cannot be accounted for simply by the relative distributions of cell types. Together, these results provide strong support for the existence of four distinct networks of parvalbumin-expressing interneurons within the basolateral nucleus.

A major distinction can be made between AC interneurons on the one hand, and DF and FS interneurons on the other. We suggest that, whereas DF and FS interneurons target perisomatic regions of postsynaptic principal neurons, axons of AC cells are likely to terminate on more distal dendrites of principal neurons. This proposal is based on several observations. First, the rise time and decay kinetics of IPSCs produced by AC interneurons were slower than those of FS and DF interneurons. We believe the most likely explanation for this is that a greater degree of electrotonic filtering occurs for AC cell IPSCs because of their more distal location from the somatic recording pipette (Miles et al., 1996; Maccaferri et al., 2000; Delaney and Sah, 2001; Pouille and Scanziani, 2004). Second, the weak, slow, but facilitating excitation received by AC interneurons is similar to that seen for dendritic interneurons in hippocampus and cortex (Beierlein et al., 2003; Pouille and Scanziani, 2004). Third, the intrinsic membrane properties of AC cells are consistent with those of other dendritic targeting interneurons. Thus, as with our AC cells, dendritic interneurons possess slower membrane time constants, exhibit spike frequency adaptation, and fire broader action potentials than their somatic counterparts (Beierlein et al., 2003; Jonas et al., 2004; Pouille and Scanziani, 2004). Furthermore, ultrastructural studies have shown that a substantial proportion (20∼28%) of PV+ terminals in the cat (Smith et al., 1998) and rat (Muller et al., 2006) basal amygdala target principal neuron distal dendrites, suggesting a similar anatomical organization of the PV+ synapses in the three species. It has also been estimated that up to 40% of calbindin-expressing interneurons in the rat basolateral nucleus, the majority of which are likely to also express parvalbumin, target distal principal neuron dendrites (Muller et al., 2003). Finally, a novel class of dendrite-targeting interneurons, which expresses the neurochemical signature of parvalbumin and calbindin coexpression, has been reported in neocortex (Blatow et al., 2003). Thus, we suggest that AC interneurons in the BLA innervate dendrites of principal neurons.

By arranging IN–IN pairs on a like/unlike basis, we showed that our putative somatic FS and DF interneurons are relatively autonomous in their connectivity, such that they preferentially form GABAergic synapses with interneurons of the same subtype. In contrast, AC interneurons, which appear to target dendrites of projection neurons, show no such preference. Because FS and DF cells preferentially inhibit interneurons of the same subtype (Fig. 7*B*), and because electrical coupling is subtype specific, communication within FS and DF networks will show a rapid GABA-mediated curtailment of the depolarizing spikelet (Fig. 4*C*). The result of this interaction is likely to be highly syn-

chronized inhibition of principal neurons by somatic FS or DF networks. In contrast, AC interneurons show no such preference for inhibiting other AC cells. Thus, the dynamics of transmission within AC networks will more closely resemble the "coupling only" scenario of Figure 4*C*, in which the spikelet is not curtailed by GABAergic inhibition. The duration of spikelet depolarization is therefore longer in networks of AC cells, such that the temporal precision with which AC networks coordinate themselves is not as great as for FS and DF networks. A similar preference for the coexistence of electrical and GABAergic synapses in somatic but not dendritic interneurons has been described for neocortical interneurons (Gibson et al., 1999). Furthermore, spikelets occurring in somatic FS interneurons have been shown to be faster than those in dendritic LTS interneurons, even in the absence of a GABAergic synapse (Gibson et al., 2005). The combination of these results suggests that the brief depolarization occurring during suprathreshold communication within somatic interneuron networks may contribute to their ability to control the temporal precision of principal neuron output.

Based on their synaptic properties and their connectivity with principal neurons and other interneurons, we suggest that FS, DF, and AC interneurons will perform different roles in BLA information processing. As seen in Figure 7*B*, DF interneurons were clearly overrepresented in reciprocally connected IN↔ PN pairs and are ideally suited for local feedback inhibition. Support for this proposed role for DF cells comes from their somatic innervation of principal neurons based on the rapid kinetics of the IPSCs they produce, and their depolarized spike threshold, which would tailor them to regulate excessive principal neuron output. Ultrastructural data showing that ~50% of somatic symmetrical synapses express parvalbumin (Muller et al., 2006) is also consistent with this proposal.

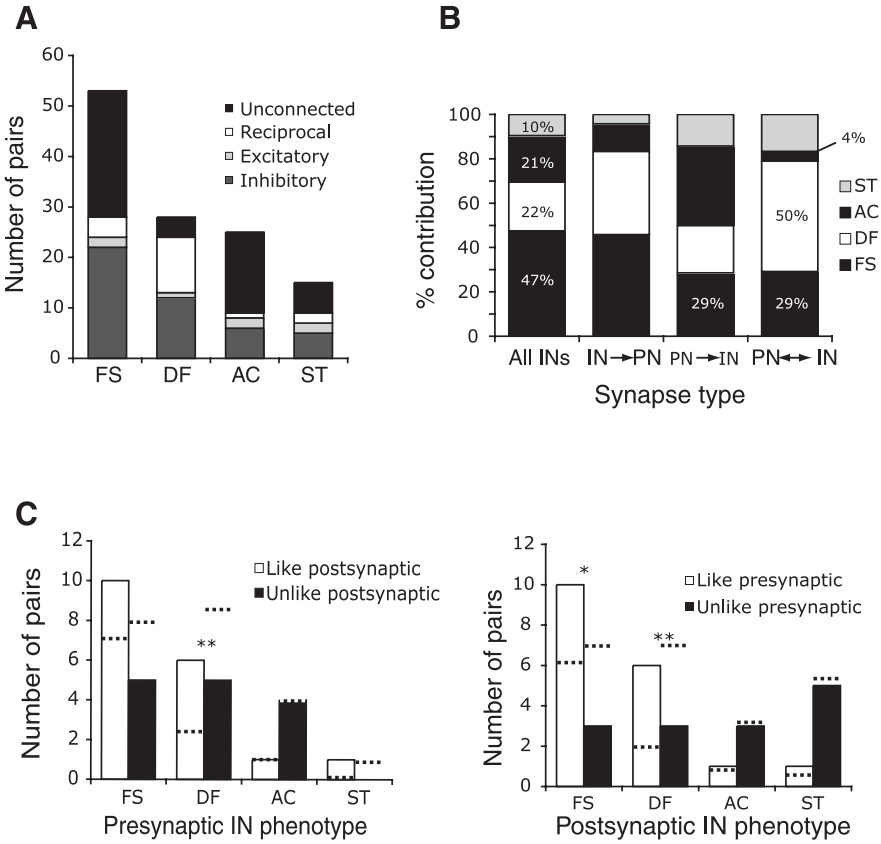

Figure 7. Connectivity principles for parvalbumin-expressing interneurons in BLA. ***A***, Chemical synaptic specificity in IN–PN pairs. The histogram shows numbers of pairs that were either unconnected (black) or connected with either a unidirectional IN→ PN connection (dark gray), unidirectional PN→ IN connection (light gray), or bidirectional PN↔ IN connection (white). ***B***, Percentage contribution of each interneuron subtype is plotted for the various forms of synaptic connection. The column on the far left shows the overall contribution of each subtype to the interneuronal population. This represents the expected value against which actual values in the other three columns are compared to determine connection specificity of IN subtypes. Percentage values in PN→IN and PN↔ IN columns represent significant deviations from chance (see text). ***C***, Synaptic specificity in IN–IN pairs. Left panel, Numbers of connected pairs with "Like" (unfilled bars) and "Unlike" (filled bars) postsynaptic partners are graphed for each presynaptic IN subtype, demonstrating selectivity in postsynaptic target selection. Right panel, As for left panel, but with postsynaptic interneuron phenotype plotted against like (white) and unlike (filled) presynaptic partners. The expected numbers of connections of each type calculated on the basis of total numbers of cell recorded (shown in leftmost column in ***B***) are shown by the dotted lines. The double asterisks mark cases where the expected values are significantly ($p < 0.01$) different from the measured values. The single asterisk marks $p < 0.05$.

In contrast, putative dendrite-targeting AC cells were almost absent from IN↔ PN pairs. Their absence from reciprocal pairs could be explained by the presumed inability of dendritic interneurons to exert a significant effect on the Na^+-dependent action potential output of principal neurons, which is likely to be somatic in origin (Miles et al., 1996). Instead, their dendritic innervation pattern would make them suitable for local feedforward inhibition of projection neuron dendrites, where they may modulate the impact of coincident excitatory inputs. Importantly, AC interneurons possess all the qualities required for delayed recruitment: slow, weak EPSCs that facilitate during repetitive activation and a slow membrane time constant (Pouille and Scanziani, 2004). Thus, the pattern of excitation required to bring AC interneurons to threshold is similar to activity patterns used to induce long-term potentiation (LTP) of excitatory synaptic inputs. We suggest that AC interneurons may therefore be ideally suited to modulating and gating the induction of LTP in the BLA.

Finally, we propose that FS interneurons may be involved in feedforward somatic inhibition of BLA principal neurons during activation of extrinsic glutamatergic afferents. This is based on the lower than expected innervation of these cells by local glutamatergic afferents (Fig. 7*B*). Although the degree of thalamic innervation of PV-interneurons in the BL is not well established, it has been reported that cortical innervation of PV-interneurons in the lateral amygdala is sparse (Smith et al., 2000). If a similar scenario held for the BLA, we would suggest that the strong glutamatergic projection from the lateral amygdala to the BLA may activate FS interneurons to evoke feedforward inhibition of BLA principal neuron somata. Feedforward somatic inhibition is thought to be crucial in enforcing temporal precision in the output of glutamatergic neurons (Pouille and Scanziani, 2001). The ability of interneurons to perform this task is dependent on a number of properties such as their rapid EPSCs, fast membrane time constants, and the reliable and fast triggering of action potentials (Jonas et al., 2004). This suggests that FS interneurons in

the BL are well suited to control the timing of principal neuron output through feedforward inhibition.

References

Bartos M, Vida I, Frotscher M, Geiger JRP, Jonas P (2001) Rapid signaling at inhibitory synapses in a dentate gyrus interneuron network. J Neurosci 21:2687–2698.

Beierlein M, Gibson JR, Connors BW (2003) Two dynamically distinct inhibitory networks in layer 4 of the neocortex. J Neurophysiol 90:2987–3000.

Berdel B, Morys J (2000) Expression of calbindin-D28k and parvalbumin during development of rat's basolateral amygdaloid complex. Int J Dev Neurosci 18:501–513.

Blatow M, Rozov A, Katona I, Hormuzdi SG, Meyer AH, Whittington MA, Caputi A, Monyer H (2003) A novel network of multipolar bursting interneurons generates theta frequency oscillations in neocortex. Neuron 38:805–817.

Davis M, Whalen PJ (2001) The amygdala: vigilance and emotion. Mol Psychiatry 6:13–34.

Delaney AJ, Sah P (2001) Pathway-specific targeting of GABA(A) receptor subtypes to somatic and dendritic synapses in the central amygdala. J Neurophysiol 86:717–723.

Freund TF, Buzaki G (1996) Interneurons of the hippocampus. Hippocampus 6:345–470.

Galarreta M, Hestrin S (1999) A network of fast-spiking cells in the neocortex connected by electrical synapses. Nature 402:72–75.

Gibson JR, Beierlein M, Connors BW (1999) Two networks of electrically coupled inhibitory neurons in neocortex. Nature 402:75–79.

Gibson JR, Beierlein M, Connors BW (2005) Functional properties of electrical synapses between inhibitory interneurons of neocortical layer 4. J Neurophysiol 93:467–480.

Gupta A, Wang Y, Markram H (2000) Organizing principles for a diversity of GABAergic interneurons and synapses in the neocortex. Science 287:273–278.

Hestrin S, Galarreta M (2005) Electrical synapses define networks of neocortical GABAergic neurons. Trends Neurosci 28:304–309.

Jonas P, Bischofberger J, Fricker D, Miles R (2004) Interneuron Diversity series: Fast in, fast out–temporal and spatial signal processing in hippocampal interneurons. Trends Neurosci 27:30–40.

Kawaguchi Y, Kondo S (2002) Parvalbumin, somatostatin and cholecystokinin as chemical markers for specific GABAergic interneuron types in the rat frontal cortex. J Neurocytol 31:277–287.

Lang EJ, Pare D (1998) Synaptic responsiveness of interneurons of the cat lateral amygdaloid nucleus. Neuroscience 83:877–889.

LeDoux JE (2000) Emotion circuits in the brain. Annu Rev Neurosci 23:155–184.

Maccaferri G, Roberts JD, Szucs P, Cottingham CA, Somogyi P (2000) Cell surface domain specific postsynaptic currents evoked by identified GABAergic neurones in rat hippocampus in vitro. J Physiol (Lond) 524:91–116.

Mahanty NK, Sah P (1998) Calcium-permeable AMPA receptors mediate long-term potentiation in interneurons in the amygdala. Nature 394:683–687.

Markram H, Toledo-Rodriguez M, Wang Y, Gupta A, Silberberg G, Wu C (2004) Interneurons of the neocortical inhibitory system. Nat Rev Neurosci 5:793–807.

Martina M, Royer S, Pare D (2001) Cell-type-specific GABA responses and chloride homeostasis in the cortex and amygdala. J Neurophysiol 86:2887–2895.

Mascagni F, McDonald AJ (2003) Immunohistochemical characterization of cholecystokinin containing neurons in the rat basolateral amygdala. Brain Res 976:171–184.

McDonald AJ (1992) Cell types and intrinsic connections of the amygdala. In: The amygdala: neurobiological aspects of emotion, memory and mental dysfunction (Aggleton JP, ed), pp 67–96. New York: Wiley.

McDonald AJ, Betette RL (2001) Parvalbumin-containing neurons in the rat basolateral amygdala: morphology and co-localization of calbindin-D(28k). Neuroscience 102:413–425.

McDonald AJ, Mascagni F (2002) Immunohistochemical characterization of somatostatin containing interneurons in the rat basolateral amygdala. Brain Res 943:237–244.

McDonald AJ, Mascagni F (2004) Parvalbumin-containing interneurons in the basolateral amygdala express high levels of the alpha1 subunit of the GABAA receptor. J Comp Neurol 473:137–146.

McDonald AJ, Mascagni F, Mania I, Rainnie DG (2005) Evidence for a perisomatic innervation of parvalbumin-containing interneurons by individual pyramidal cells in the basolateral amygdala. Brain Res 1035:32–40.

Meyer AH, Katona I, Blatow M, Rozov A, Monyer H (2002) *In vivo* labeling of parvalbumin-positive interneurons and analysis of electrical coupling in identified neurons. J Neurosci 22:7055–7064.

Miles R, Toth K, Gulyas AI, Hajos N, Freund TF (1996) Differences between somatic and dendritic inhibition in the hippocampus. Neuron 16:815–823.

Muller JF, Mascagni F, McDonald AJ (2003) Synaptic connections of distinct interneuronal subpopulations in the rat basolateral amygdalar nucleus. J Comp Neurol 456:217–236.

Muller JF, Mascagni F, McDonald AJ (2005) Coupled networks of parvalbumin-immunoreactive interneurons in the rat basolateral amygdala. J Neurosci 25:7366–7376.

Muller JF, Mascagni F, McDonald AJ (2006) Pyramidal cells of the rat basolateral amygdala: synaptology and innervation by parvalbumin-immunoreactive interneurons. J Comp Neurol 494:635–650.

Pouille F, Scanziani M (2001) Enforcement of temporal fidelity in pyramidal cells by somatic feed-forward inhibition. Science 293:1159–1163.

Pouille F, Scanziani M (2004) Routing of spike series by dynamic circuits in the hippocampus. Nature 429:717–723.

Rainnie DG, Asprodini EK, Shinnick-Galalgher P (1993) Intracellular recordings from morphologically identified neurons of the basolateral amygdala. J Neurophysiol 69:1350–1362.

Rainnie DG, Mania I, Mascagni F, McDonald AJ (2006) Physiological and morphological characterization of parvalbumin-containing interneurons of the rat basolateral amygdala. J Comp Neurol 498:142–161.

Sah P, Faber ES, Lopez De Armentia M, Power J (2003) The amygdaloid complex: anatomy and physiology. Physiol Rev 83:803–834.

Smith Y, Paré JF, Paré D (1998) Cat intraamygdaloid inhibitory network: ultrastructural organization of parvalbumin-immunoreactive elements. J Comp Neurol 391:164–179.

Smith Y, Paré JF, Paré D (2000) Differential innervation of parvalbumin-immunoreactive interneurons of the basolateral amygdaloid complex by cortical and intrinsic inputs. J Comp Neurol 416:496–508.

Sosulina L, Meis S, Seifert G, Steinhauser C, Pape HC (2006) Classification of projection neurons and interneurons in the rat lateral amygdala based upon cluster analysis. Mol Cell Neurosci 33:57–67.

Washburn MS, Moises HC (1992) Electrophysiological and morphological properties of rat basolateral amygdaloid neurons *in vitro*. J Neurosci 12:4066–4079.

Yoshimura Y, Callaway EM (2005) Fine-scale specificity of cortical networks depends on inhibitory cell type and connectivity. Nat Neurosci 8:1552–1559.

Yoshimura Y, Dantzker JL, Callaway EM (2005) Excitatory cortical neurons form fine-scale functional networks. Nature 433:868–873.